ADVANCED FUNCTIONAL MATERIALS
www.afm-journal.de

Materials Views
www.MaterialsViews.com

High Efficiency White Organic Light-Emitting Devices Incorporating Yellow Phosphorescent Platinum(II) Complex and Composite Blue Host

*Shiu-Lun Lai, Wai-Yip Tong, Steven C. F. Kui, Mei-Yee Chan, Chi-Chung Kwok, and Chi-Ming Che**

A new class of charge neutral, strongly luminescent cyclometalated platinum(II) complexes supported by dianionic tetradentate ligand are synthesized. One of these platinum(II) complexes, Y-Pt, displays a high photoluminescence quantum yield of 86% and electroluminescence efficacy (η_{power}) of up to 52 lm W^{-1}, and is utilized as a yellow phosphorescent dopant in the fabrication of white organic light-emitting devices (WOLEDs). WOLEDs based on conventional structures with yellow emission from Y-Pt in combination with blue emission from *bis*(4,6-difluorophenyl-pyridinato-*N*,$C^{2'}$) (picolinate) iridium(III) (FIrpic) show a total η_{power} of up to 31 lm W^{-1}. A two-fold increase in η_{power} by utilizing a modified WOLED structure comprising of a composite blue host is realized. With this modified device structure, the total η_{power} and driving voltage at a luminance of 1000 cd m^{-2} can be improved to 61 lm W^{-1} and 7.5 V (i.e., 10 V for control devices). The performance improvement is attributed to an effectively broaden exciton formation-recombination zone and alleviation of localized exciton accumulation within the FIrpic-doped composite host for reduced triplet-triplet annihilation, yielding blue light-emission with enhanced intensity. The modified device structure can also adopt a higher concentration of Y-Pt towards its optimal value, leading to WOLEDs with high efficiency.

1. Introduction

Since the accomplishment of white organic light-emitting devices (WOLEDs) with over 30 lm W^{-1} of luminous efficiency (η),[1–4] WOLEDs with high η have been receiving immense attention as next-generation illumination alternatives to existing incandescent bulbs and fluorescent tubes. In this area, the development of new smart functional materials and novel device architectures is crucial to realize practical WOLED technology.[1–8] Recently, a record-high total efficacy of 110 lm W^{-1} from WOLED prototypes utilizing red-green-blue (RGB) phosphors in the emissive layers and equipped with advanced light out-coupling enhancement components has been reported by Reineke et al.[2]

Apart from the RGB approach, white light can be obtained via the combination of complementary emission colors, i.e., either blue and yellow (BY) or blue and red (BR). With only two emitters used for white light emission, the device structure is greatly simplified. More importantly, the correlated color temperature (CCT) of white light emission (i.e., cool or warm white) can be precisely and easily adjusted via manipulating the ratio of blue to yellow/red emitters (phosphorescent dopants). Indeed, WOLEDs comprising newly developed blue and yellow metal-organic phosphors of *mer-tris*(*N*-dibenzofuranyl-*N'*-methylimidazole) iridium(III) [Ir(dbfmi)] and *bis*(2-phenylbenzothiazolato)(acetylacetonate) iridium(III) [BT_2Ir(acac)] with high power efficiencies (η_{power}) of 60 lm W^{-1} have recently been demonstrated by Kido's group without the use of any light out-coupling enhancement technique.[3] Although yellow emission is a key parameter in the BY approach, unlike fluorescent materials, research efforts towards the design and synthesis of efficient yellow phosphorescent materials are sparse when compared to the efforts made to the development of new materials which emit monochromatic primary RGB colors. Meanwhile, for blue phosphorescent materials, due to their intrinsically wide band-gap and large triplet energy (T_1) of over 2.5 eV, the carrier transport from the respective electrodes into emitting phosphor doped host material and the subsequent energy transfer from host material to blue phosphor are inherently less efficient. This poses a bottleneck on η of WOLEDs based on this BY (or BR) approach. Up to now, the η values of the commercially available blue phosphors are much lower than that of yellow and red counterparts. For instance, η_{power} of the typical blue *bis*(4,6-difluorophenyl-pyridinato-*N*,$C^{2'}$) (picolinate) iridium(III) (FIrpic) is only 24 lm W^{-1},[9] while

Dr. S.-L. Lai, W.-Y. Tong, Dr. S. C. F. Kui, Dr. M.-Y. Chan, Dr. C.-C. Kwok, Prof. C.-M. Che
State Key Laboratory of Synthetic Chemistry
HKU-CAS Joint Laboratory on New Materials
Department of Chemistry
The University of Hong Kong
Pokfulam Road, Hong Kong
E-mail: cmche@hku.hk

DOI: 10.1002/adfm.201300281

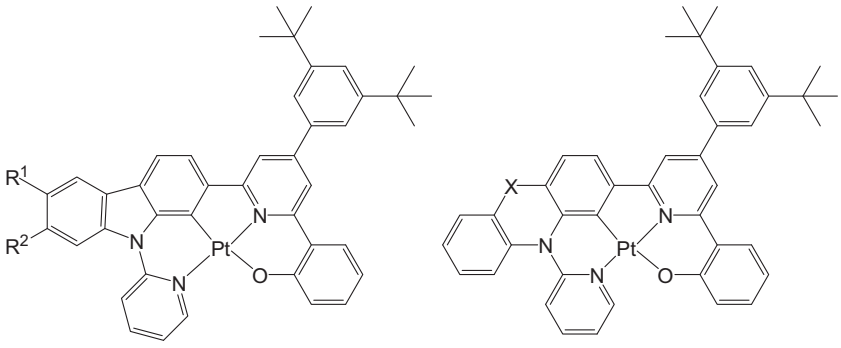

Scheme 1. Chemical structures of complexes **1**–**5**.

those of yellow *bis*(2-phenyl-6-fluorobenzothiozolato) (acetylacetonate) iridium(III) [$(F\text{-}bt)_2Ir(acac)$][4] and red *bis*-(2-phenylquinolyl-$N,C^{2'}$) (acetylacetonate) iridium(III) (PQIr)[10] emitters are 45 and 43 lm W^{-1}, respectively, at their optimized doping concentrations of 5–15%. In order to achieve good chromaticity of white light, excessive yellow (or red) emission should be inevitably sacrificed to balance the blue emission, resulting in poor η for such WOLEDs. This accounts for a relatively low doping concentration (≤3%) of yellow (or red) phosphor to be always used in these two-component WOLEDs.[3–6]

Herein we report the fabrication of WOLEDs using a modified device architecture that can improve the η_{power} without sacrifice of white color balance. The devices based on a composite blue host doped with 8% FIrpic and a homogenous yellow host doped with 4% of a newly synthesized organoplatinum(II) complex (**Y-Pt**) showed a two-fold increase in η_{power} from 18 lm W^{-1} with the employment of conventional structure to 36 lm W^{-1} (i.e., equivalent to the total η_{power} from 31 lm W^{-1} to 61 lm W^{-1}) without the need to use any light outcoupling technique. At the same time, the operational voltage at 1000 cd m^{-2} can be significantly reduced from 10 V for the control devices to 7.5 V for the modified devices. The mechanism accounting for the improvement in device performance has been elaborated.

2. Results and Discussion

2.1. Synthesis and Characterization of Y-Pt

A new series of robust cyclometalated platinum(II) complexes supported by the rigid tetradentate O^N^C^N ligands, **1**–**5** (**Scheme 1**), were synthesized and characterized. The substitution pattern of O^N^C^N ligand is observed to alter both the thermal and photophysical properties of the platinum(II) complexes. **Figure 1**a shows the thermogravimetric curves of **1**–**5** measured under a constant heating rate of 10 °C min^{-1} at ambient conditions. Due to the strong chelation effect of O^N^C^N ligands, these complexes are thermally stable with high decomposition temperature (i.e., T_d corresponds to 5% weight loss in thermogravimetric analysis (TGA) measurement) of 304–410 °C. Figure 1b shows the absorption (Abs) and photoluminescence (PL) spectra of **1**–**5** in degassed dichloromethane solutions (2.0×10^{-5} mol dm^{-3}) at 298 K. An intense vibronic-structured absorption band at wavelength below 350 nm with molar absorption coefficients (ε) ≈ $1.5–5.3 \times 10^4$ dm^3 mol^{-1} cm^{-1} is attributed to intraligand (IL) [$\pi \rightarrow \pi^*$] transitions of O^N^C^N ligand. In addition, there is a less intense absorption band at >400 nm with $\varepsilon \approx <10^4$ dm^3 mol^{-1} cm^{-1}. This low-energy absorption band is tentatively assigned to mixed IL π–π^* and metal-to-ligand charge transfer transitions. Meanwhile, the PL spectra of **1**–**5** exhibit emissions from saturated green to yellow with peak maxima (λ_{PL}) at ca. 526–553 nm and with high luminescence quantum yields (Φ_L) of 47–86% and emission lifetimes (τ) of 5.9–8.8 μs in solutions. Such high Φ_L of the complexes can be ascribed to the rigidity of the O^N^C^N ligand upon coordination to Pt(II) ion. The vibrational spacings of ca. 1300 cm^{-1}, which correspond to the C = C/C = N skeletal stretchings, are in accordance with the spectral assignment of the emissions to come from triplet excited states with predominant ligand character. It is noted that this class of platinum(II) complexes are coordinated by only one ligand and hence they are in principle more advantageous in the context of thermal stability than those metal complexes coordinated with two bidentate ligands or with a tridentate ligand plus an

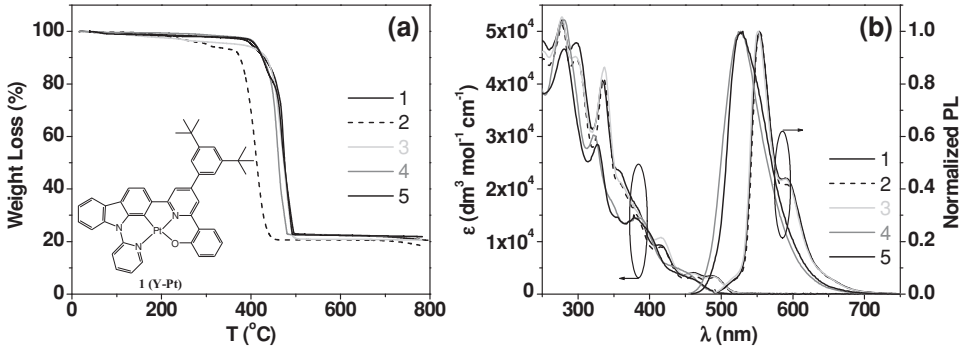

Figure 1. a) Thermogravimetric curves of complexes **1**–**5** under a constant heating rate of 10 °C min^{-1}. Inset: Molecular structure of **Y-Pt** (complex **1**). b) UV-vis absorption and emission spectra of complexes **1**–**5** in dichloromethane solutions at 298 K.

Table 1. Photophysical data of complexes **1**–**5**.

	UV–vis absorption[a] λ_{max} [nm] (ε [$\times 10^4$ dm^3 mol^{-1} cm^{-1}])	λ_{PL} [nm] (τ [μs])[a]	Φ_L [%][b]	T_d [°C][c]
1 (Y-Pt)	277 (5.21), 298 (4.78), 334 (4.07), 358 (2.34), 418 (0.92), 461 (0.41), 488 (0.35)	553 (6.6), 587 (6.8)	86	400
2	278 (5.12), 298 (4.48), 336 (4.10), 358 (2.11), 415 (0.90), 460 (0.34), 487 (0.32)	553 (7.4), 590 (7.2)	67	304
3	278 (5.27), 296 (4.52), 337 (4.32), 360 (2.12), 416 (1.08), 462 (0.39), 486 (0.34)	552 (8.0), 590 (7.6)	82	372
4	280 (5.22), 322 (3.03), 385 (1.46), 443 (sh, 0.47)	526 (5.9)	47	410
5	281 (4.67), 327 (2.85), 354 (1.46), 379 (1.45), 453 (sh, 0.32)	527 (8.8)	49	409

[a]In degassed dichloromethane solutions (2.0×10^{-5} mol dm^{-3}); [b]In degassed dichloromethane solutions (2.0×10^{-5} mol dm^{-3}) by the optical dilute method with $[Ru(bpy)_3](PF_6)_2$ (bpy = 2,2′-bipyridine) in degassed acetonitrile solution ($\Phi_{ref} = 0.062$) for complexes **1**–**3** or 9,10-*bis*(phenylethynyl)anthracene in benzene solution ($\Phi_{ref} = 0.96$) for complexes **4** and **5** as a reference standard; [c]5% weight loss in TGA measurement.

ancillary ligand, such as $(C^N)_2Ir(L)$, where C^N is 2-phenylpyridine and its derivatives, and L is acetylacetonate (acac) or picolinate (pic). The photophysical data of **1**–**5** are summarized in **Table 1**. Among these complexes, **Y-Pt** (i.e., compound **1**) was chosen as a yellow phosphorescent emitter (dopant) for our BY-type WOLEDs due to its superior luminescent properties[11–14] and FIrpic was chosen as the blue phosphorescent emitter (dopant) because it is commercially accessible possessing high η. **Table 2** compares the thermal, photophysical and electroluminescence (EL) properties of **Y-Pt** with those of the reported yellow phosphorescent emitters. It is noted that η_{power} of the **Y-Pt**-based devices can achieve over 50 lm W^{-1}. Notably, the overall performance in terms of Φ_L and η_{power} of **Y-Pt** is comparable to those of the best reported iridium(III)[4,5,15–19] or even better than those of platinum(II)[12,13,20,21] based yellow light-emitting phosphors.

Figure 2 depicts the schematic energy level diagrams of the fabricated OLEDs. All data of T_1, lowest unoccupied molecular orbital (LUMO) and highest occupied molecular orbital (HOMO) levels of organic materials,[6,22,23] and work functions of LiF/Al[6] and ITO/molybdenum(VI) oxide (MoO_x)[24] were extracted from the literature. In the figures, NPB, mCP, UGH2, BAlq, TAZ, and TCTA denote for 4,4′-*bis*-(1-naphthyl-*N*-phenylamino)-biphenyl, *N,N*′-dicarbazolyl-3,5-benzene, *p-bis*(triphenylsilyly)benzene, *bis*(2-methyl-8-quinolinato)(4-phenylphenolate)aluminium(III), 3-(4-biphenyl)-4-phenyl-5-(4-*tert*-butylphenyl)-1,2,4-triazole, and 4,4′,4″-*tris*(*N*-carbazolyl)-triphenylamine, respectively. It is highlighted that T_1 of the chosen phosphorescent hosts, i.e., TCTA, mCP, UGH2, are higher in energy than that of the blue FIrpic and yellow **Y-Pt** phosphors respectively, in order to ensure effective exothermic energy transfer and to prevent undesirable backward energy transfer from guest phosphor molecules to the hosts. In addition, the stepped progression of both the closely spaced HOMO and LUMO levels forms a cascade type energy band structure that favors effective charge transport from respective electrodes into the emissive layers.

2.2. EL Characteristics of Monochrome OLEDs Based on FIrpic and Y-Pt

Two sets of monochrome OLEDs with structures of ITO/NPB (40 nm)/mCP (10 nm)/x% FIrpic:UGH2 (20 nm)/BAlq (40 nm)/LiF (0.5 nm)/Al (80 nm) for blue emission from FIrpic and ITO/NPB (40 nm)/y% **Y-Pt**:mCP (30 nm)/BAlq (40 nm)/LiF (0.5 nm)/Al (80 nm) for yellow emission from **Y-Pt** were fabricated. **Figure 3** shows the normalized EL spectra of the FIrpic and **Y-Pt** devices. The EL spectrum of FIrpic device was independent of dopant concentration with an EL peak maximum (λ_{EL}) at 472 nm. On the other hand, λ_{EL} of the **Y-Pt** device with 2% **Y-Pt** was at 562 nm. This λ_{EL} showed a slight red-shift

Table 2. Thermal, photophysical, and EL properties for some yellow phosphorescent emitters recently reported in the literature.

Emitter (Category)	Conc. [%][a]	T_d [°C][b]	Solution Φ_L [%]	Max. η_{power} [lm W^{-1}]	λ_{EL} [nm]	FWHM [nm, cm^{-1}]	CIE x, y
Y-Pt [This work]	6	400	86	52.1	568	76, 2207	0.52, 0.47
2 ((R^C^N^N)PtCl)[13]	6	471	68	23.2	540	82, 2555	0.44, 0.54
$Pt(L^3)$[12]	5	325	27	14.0	555	89, 2666	0.48, 0.52
(F-bt)Pt(acac)[20]	5	249	–	6.6	577	125, 3701	0.47,0.50
$Pt(ptp)_2$[21]	45	–	–	2.4	570	103, 3202	0.44, 0.51
$(F\text{-}bt)_2Ir(acac)$[4]	5	338	32	44.9	562	79, 2339	0.50, 0.49
p-PF-py[16]	6	–	–	29.0	559	72, 2233	—
$Ir(npy)_2acac$[15]	6	–	22	21.8	551	87, 2689	0.45, 0.54
2 ($(C^N)_2Ir(acac)$)[5]	15	502	12	13.4	560	66, 1982	0.49, 0.50
C1 ($(C^N)_2Ir(acac)$)[17]	10	460	52	12.7	550	63, 1955	0.47, 0.53
$(fbi)_2Ir(acac)$[18]	6	–	51	11.4	568	68, 1980	0.51, 0.48
$Ir(2\text{-}PhPyCz)_2(acac)$[19]	7	–	–	5.0	556	71, 2160	0.48, 0.53

[a]Optimized concentration for attaining maximum EL efficiency; [b]5% weight loss in TGA measurement.

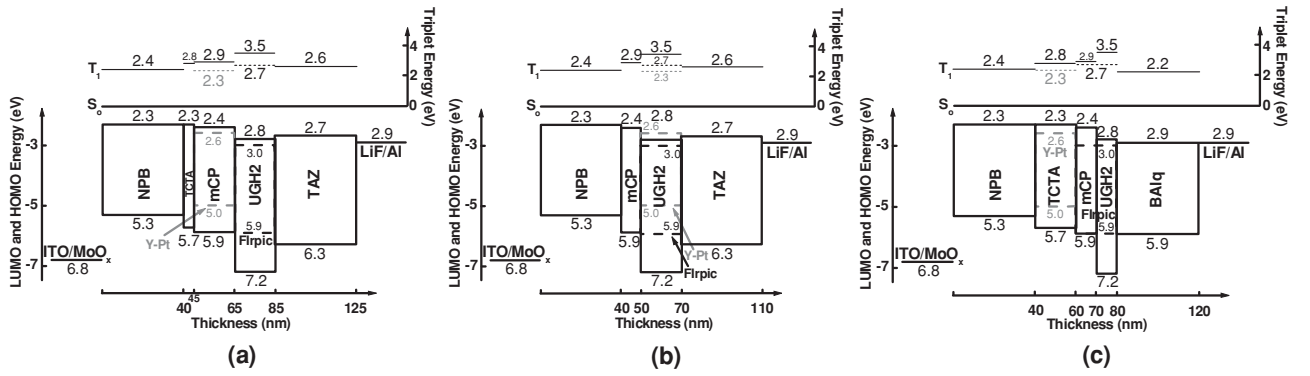

Figure 2. Schematic energy level diagrams of the WOLEDs with configurations a) ITO/MoO_x (5 nm)/NPB (40 nm)/TCTA (5 nm)/**Y-Pt**:mCP (20 nm)/FIrpic:UGH2 (20 nm)/TAZ (40 nm)/LiF (0.5 nm)/Al (100 nm), b) ITO/MoO_x (5 nm)/NPB (40 nm)/mCP (10 nm)/**Y-Pt**:FIrpic:UGH2 (20 nm)/TAZ (40 nm)/LiF (0.5 nm)/Al (100 nm), and c) ITO/MoO_x (5 nm)/NPB (40 nm)/**Y-Pt**:TCTA (20 nm)/FIrpic:mCP (10 nm)/FIrpic:UGH2 (10 nm)/BAlq (40 nm)/LiF (0.5 nm)/Al (100 nm). LUMO and HOMO are the lowest unoccupied molecular orbital and the highest occupied molecular orbital, respectively.

in energy (≤10 nm) with the EL spectrum became broadened upon increasing **Y-Pt** dopant concentration. The full spectral width at half maximum (FWHM) increased from 65 nm in the case of the 2% **Y-Pt** device to 80 nm for the 8% **Y-Pt** device. The corresponding Commission Internationale de L'Eclairage (CIE) coordinates for 8% FIrpic and 6% **Y-Pt** are (0.16, 0.32) and (0.52, 0.47), respectively. Such broad EL spectra of **Y-Pt** devices are beneficial for attaining a better white color in combination with blue color. It is noted that an additional peak at ca. 468 nm originated from BAlq emission was observed for the 2% **Y-Pt** device. This unwanted blue emission is attributed to inefficient charge trapping on guest **Y-Pt** molecules and hence the occurrence of exciton recombination within the electron-transporting layer (ETL), i.e., BAlq, at a low dopant concentration of 2% **Y-Pt**. **Figure 4** depicts the current efficiency ($\eta_{current}$) and η_{power} of FIrpic and **Y-Pt** OLEDs as a function of dopant concentration. At an optimized concentration of 8% FIrpic, the device exhibited maximum $\eta_{current}$ of 28.5 cd A^{-1} and η_{power} of 25.6 lm W^{-1} while those of 6% **Y-Pt** are 74.9 cd A^{-1} and 52.1 lm W^{-1}. Further increase in dopant concentration led to severe efficiency roll-off, and this is attributed to an increase in the number of nonradiative pathways available to the triplet excitons of the dopant aggregates, i.e., concentration induced quenching, and the enhanced triplet percolation between adjacent or clustered dopant molecules, i.e., triplet-triplet annihilation.[25]

2.3. WOLEDs with Conventional Structures

As η_{power} for FIrpic device can reach only half of that of **Y-Pt** device, we prepared WOLED structure with the optimized concentration of FIrpic at 8% aiming to harvest the largest contribution of blue emission. Two sets of WOLEDs with commonly used configurations have been fabricated,[6,23,26] in which the

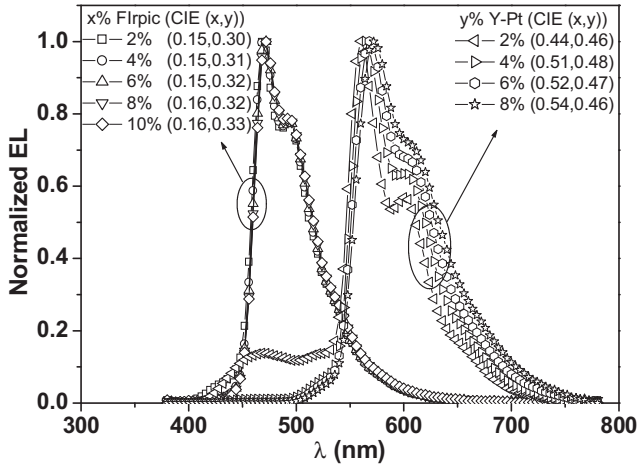

Figure 3. Normalized EL spectra of monochromatic blue and yellow OLEDs with basic configurations ITO/NPB (40 nm)/mCP (10 nm)/x% FIrpic:UGH2 (20 nm)/BAlq (40 nm)/LiF (0.5 nm)/Al (80 nm) for blue and ITO/NPB (40 nm)/y% **Y-Pt**:mCP (30 nm)/BAlq (40 nm)/LiF (0.5 nm)/Al (80 nm) for yellow, where x is 2, 4, 6, 8, 10 and y is 2, 4, 6, 8. CIE (x,y) represents the Commission Internationale de L'Eclairage coordinates.

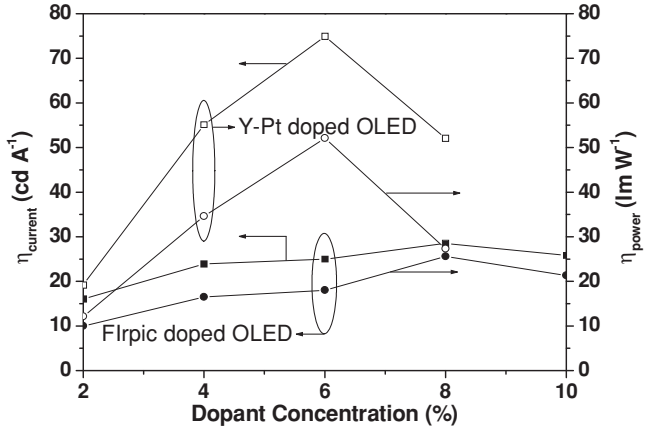

Figure 4. Current and power efficiencies ($\eta_{current}$ and η_{power}) as a function of dopant concentration of the FIrpic-based blue OLEDs and the **Y-Pt**-based yellow OLEDs, respectively.

Table 3. Characteristics of WOLEDs. $V_{turn\text{-}on}$, $\eta_{current}$, η_{power}, η_{EQE} are the turn-on voltage, current, power and external quantum efficiencies, respectively.

Conc. (y)	η_{power}@ Max/100 cd m^{-2}/ 1000 cd m^{-2}/Total [lm W^{-1}]	$\eta_{current}$@ Max/100 cd m^{-2}/ 1000 cd m^{-2} [cd A^{-1}]	η_{EQE}@ Max/100 cd m^{-2}/ 1000 cd m^{-2} [%]	$V_{turn\text{-}on}$ [V]	V@ 100 cd m^{-2}/ 1000 cd m^{-2} [V]	V@ 20 mA cm^{-2} [V]	CIE [x,y]@ 10 cd m^{-2}
1.0%[a)]	13.9/9.7/1.5/23.6	20.5/17.7/4.8	8.6/7.6/2.0	4.2	5.7/10.3	10.2	0.24,0.39
2.0%[a)]	18.0/11.5/1.9/30.6	26.8/21.7/6.2	10.0/8.3/2.4	4.3	5.9/10.3	10.7	0.33,0.43
3.0%[a)]	19.7/12.8/2.5/33.5	29.8/24.3/8.0	10.3/8.6/2.9	4.3	6.0/10.1	11.0	0.40,0.46
4.0%[a)]	18.5/12.9/2.7/31.5	29.6/25.5/8.8	10.0/8.8/3.1	4.3	6.2/10.4	11.4	0.44,0.47
0.5%[b)]	17.8/10.6/1.4/30.3	24.4/19.2/4.5	9.0/7.3/1.8	4.1	5.8/10.0	9.8	0.30,0.42
1.0%[b)]	19.1/11.3/1.6/32.5	26.0/20.7/5.1	9.0/7.2/1.9	4.1	5.9/10.0	10.0	0.35,0.45
2.0%[b)]	21.3/11.2/1.8/36.2	28.5/21.8/6.0	9.1/7.0/2.0	4.2	6.2/10.4	10.7	0.43,0.49
3.0%[b)]	19.0/10.4/1.9/32.3	26.7/20.7/6.5	8.9/6.7/2.2	4.3	6.3/10.5	10.9	0.47,0.49
1.0%[c)]	23.4/17.4/5.1/39.8	33.5/29.0/12.1	14.2/12.9/5.6	3.4	5.2/7.4	8.5	0.22,0.38
2.0%[c)]	26.3/19.2/5.9/44.7	37.7/32.0/14.0	15.0/13.4/6.1	3.3	5.2/7.4	8.7	0.26,0.41
3.0%[c)]	29.9/19.7/6.4/50.8	40.4/33.0/15.1	15.4/13.4/6.4	3.2	5.3/7.5	8.9	0.29,0.42
4.0%[c)]	35.8/21.6/6.9/60.9	45.6/36.2/16.4	16.0/14.1/6.7	3.2	5.3/7.5	9.0	0.34,0.44

[a)]ITO/MoO_x (5 nm)/NPB (40 nm)/TCTA (5 nm)/y% **Y-Pt**:mCP(20 nm)/8% FIrpic:UGH2 (20 nm)/TAZ (40 nm)/LiF (0.5 nm)/Al (100 nm); [b)]ITO/MoO_x (5 nm)/NPB (40 nm)/mCP(10 nm)/y% **Y-Pt**:8% FIrpic:UGH2 (20 nm)/TAZ (40 nm)/LiF (0.5 nm)/Al (100 nm); [c)]ITO/MoO_x (5 nm)/NPB (40 nm)/y% **Y-Pt**:TCTA (20 nm)/8% FIrpic:mCP(10 nm)/8% FIrpic:UGH2 (10 nm)/BAlq (40 nm)/LiF (0.5 nm)/Al (100 nm).

blue dopant and yellow dopant were separately doped into different host materials of UGH2 and mCP [i.e., ITO/MoO_x (5 nm)/NPB (40 nm)/TCTA (5 nm)/y% **Y-Pt**:mCP (20 nm)/8% FIrpic:UGH2 (20 nm)/TAZ (40 nm)/LiF (0.5 nm)/Al (100 nm)] (*hereafter denoted as B/Y devices*), or doped into a single host of UGH2 [i.e., ITO/MoO_x (5 nm)/NPB (40 nm)/mCP (10 nm)/y% **Y-Pt**:8% FIrpic:UGH2 (20 nm)/TAZ (40 nm)/LiF (0.5 nm)/Al (100 nm)] (hereafter denoted as B:Y devices). Dopant concentration of **Y-Pt** was varied in order to fine tune the chromaticity of white light for both types of WOLEDs. The key parameters of WOLEDs are summarized in **Table 3**. For B/Y device, white light with CIE coordinates of (0.33, 0.43) was obtained when 2% **Y-Pt** was used. Its maximum η_{power}, $\eta_{current}$, and external quantum efficiency (η_{EQE}) were 18 lm W^{-1} (equivalent to a total η_{power} = 31 lm W^{-1}), 26.8 cd A^{-1} and 10% photons electron^{-1}, respectively. On the other hand, the B:Y device achieved similar CIE coordinates of (0.35, 0.45) with a lower **Y-Pt** concentration (i.e., 1%). As both B/Y and B:Y devices had similar EL color coordinates, the difference in the **Y-Pt** concentrations used in these two devices could be attributed to an additional energy transfer pathway from the blue FIrpic to the yellow **Y-Pt** phosphors. Thus, in the case of the B:Y device, this led to excessive yellow emission and hence a lower **Y-Pt** concentration could be used to maintain color balance/white chromaticity. This effect is particularly incurred in WOLEDs with RGB or BY emitters simultaneously co-doped into a wide energy gap host, in which case the majority of excitons are trapped on blue dopant present at high concentration, and subsequent energy transfer to the green-red or yellow dopant present at low concentration to give a broad spectral white light emission.[27] Interestingly, the performance of B:Y devices were almost identical to that of B/Y WOLEDs with their maximum η_{power}, $\eta_{current}$, and η_{EQE} being 19.1 lm W^{-1}, 26 cd A^{-1}, and 9%, respectively. However, the driving voltages were both 10 V at luminance of 1000 cd m^{-2} and at current density of 20 mA cm^{-2}, while those of the B/Y devices were 10.3 and 10.7 V, respectively. The voltage drop under a constant current density is assigned to the reduction in total film thickness or cell resistance.

In order to achieve good white chromaticity, the concentrations of the yellow phosphor, **Y-Pt**, in both types of WOLEDs have to be low, i.e., 1–2%. This finding is in good agreement with other reported studies.[3–6] As reported by Sun et al.[1] and Wang et al.,[23] η of WOLED (η_{WOLED}) is governed by η of monochromatic blue and yellow OLEDs (i.e., η_{blue} and η_{yellow}) and the fraction of excitons trapped and formed on the phosphor dopants in the emissive layers (χ_{Trap}), and is given by Equation 1:

$$\eta_{WOLED} = (1 - \chi_{Trap})\eta_{blue} + \chi_{Trap}\eta_{yellow} \quad (1)$$

In short, η_{WOLED} is governed by both η_{blue} and η_{yellow}. The rather low concentration of **Y-Pt** (i.e., far away from its optimized value of 6%) inevitably leads to lowering of the η_{yellow}, and hence the η_{WOLED}.

2.4. WOLEDs Incorporating a Composite Blue Host

To overcome the issue mentioned in the previous section, WOLEDs with a modified configuration of ITO/MoO_x (5 nm)/NPB (40 nm)/y% **Y-Pt**:TCTA (20 nm)/8% FIrpic:mCP(10 nm)/8% FIrpic:UGH2 (10 nm)/BAlq (40 nm)/LiF (0.5 nm)/Al (100 nm) were fabricated (hereafter denoted as B/B/Y devices). This structure was composed of a heterogeneous blue host layer (i.e., slabs of mCP and UGH2) uniformly doped with 8% FIrpic. As expected, the peak η of 2% **Y-Pt** B/B/Y device was increased to 26.3 lm W^{-1} and 37.7 cd A^{-1}, although the relative intensity of blue emission was higher. As depicted in Table 3, this led to a poor white light chromaticity with CIE coordinates of (0.26, 0.41). Upon increasing the **Y-Pt** concentration up to 4%, η could be further increased up to 35.8 lm W^{-1}

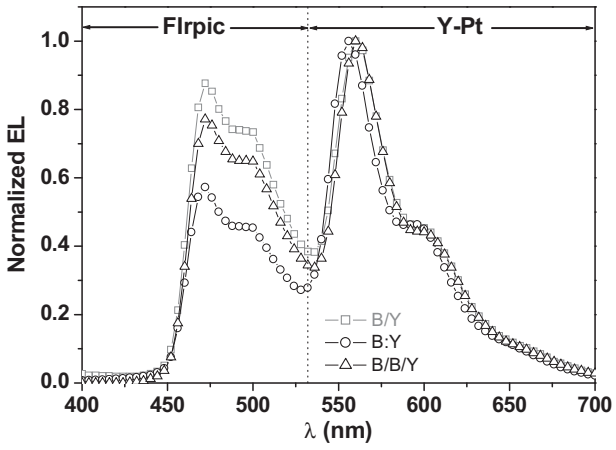

Figure 5. Normalized EL spectra of WOLEDs with the structures of ITO/MoO_x (5 nm)/NPB (40 nm)/TCTA (5 nm)/2% **Y-Pt**:mCP (20 nm)/8% FIrpic:UGH2 (20 nm)/TAZ (40 nm)/LiF (0.5 nm)/Al (100 nm) (□), ITO/MoO_x (5 nm)/NPB (40 nm)/mCP (10 nm)/1% **Y-Pt**:8% FIrpic:UGH2 (20 nm)/TAZ (40 nm)/LiF (0.5 nm)/Al (100 nm) (○), and ITO/MoO_x (5 nm)/NPB (40 nm)/4% **Y-Pt**:TCTA (20 nm)/8% FIrpic:mCP (10 nm)/8% FIrpic:UGH2 (10 nm)/BAlq (40 nm)/LiF (0.5 nm)/Al (100 nm) (△).

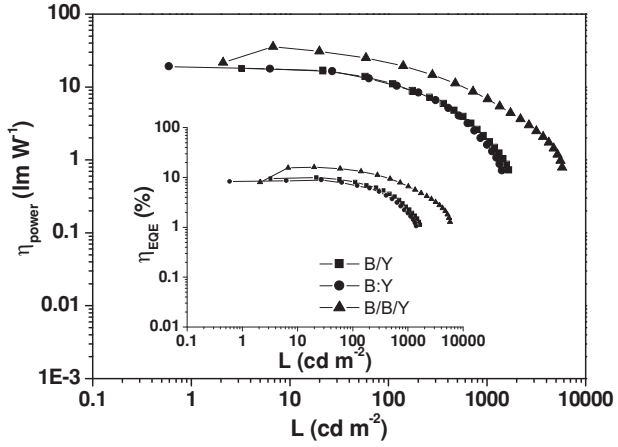

Figure 6. η_{power} (Inset: η_{EQE}) as a function of luminance of the WOLEDs. Device structures: ITO/MoO_x (5 nm)/NPB (40 nm)/TCTA (5 nm)/2% **Y-Pt**:mCP (20 nm)/8% FIrpic:UGH2 (20 nm)/TAZ (40 nm)/LiF (0.5 nm)/Al (100 nm) (□); ITO/MoO_x (5 nm)/NPB (40 nm)/mCP (10 nm)/1% **Y-Pt**:8% FIrpic:UGH2 (20 nm)/TAZ (40)/LiF (0.5 nm)/Al (100 nm) (○); and ITO/MoO_x (5 nm)/NPB (40 nm)/4% **Y-Pt**:TCTA (20 nm)/8% FIrpic:mCP (10 nm)/8% FIrpic:UGH2 (10 nm)/BAlq (40 nm)/LiF (0.5 nm)/Al (100 nm) (△).

(equivalent to a total η_{power} = 61 lm W^{-1}), 45.6 cd A^{-1}, and 16%. The η_{power} was increased by two-fold when compared to that of 2% **Y-Pt** B/Y device (i.e., η_{power} of 18 lm W^{-1} and total η_{power} of 31 lm W^{-1}). Meanwhile, its chromaticity was significantly improved with CIE coordinates of (0.34, 0.44) and an average color rendering index (CRI) of 60 was calculated from the EL spectra according to the CIE CRI method.[28] **Figure 5** depicts the normalized EL spectra of 2% **Y-Pt** B/Y, 1% **Y-Pt** B:Y, and 4% **Y-Pt** B/B/Y devices viewed in the normal direction at a luminance of 10 cd m^{-2}. The EL spectra of the WOLEDs resemble to the summation of the emission spectra of FIrpic and **Y-Pt** that covers the spectral region from 450 to 700 nm. **Figure 6** depicts the plots of η_{power} and η_{EQE} (inset of Figure 6) as a function of luminance of WOLEDs. Unlike the other WOLEDs with conventional structures, i.e., B/Y or B:Y that η sharply decreases at high brightness/current density due to declining charge balance and triplet exciton quenching, the present WOLEDs with the modified structure showed a less pronounced η roll-off. This smaller η roll-off for the modified B/B/Y device is attributed to reduced triplet-triplet annihilation.[25]

As revealed by the current density–voltage–luminance (*J–V–L*) characteristics of WOLEDs depicted in **Figure 7**, the turn-on voltage ($V_{turn\text{-}on}$), defined as the smallest voltage to realize measurable luminance of 1 cd m^{-2}, and the operating voltages to obtain a luminance of 1000 cd m^{-2} and a current density of 20 mA cm^{-2} all of which were significantly decreased from 4.3, 10.3, and 10.7 V for the 2% **Y-Pt** B/Y device to only 3.2, 7.5, and 9.0 V, respectively, for the modified 4% **Y-Pt** B/B/Y device. These comparatively low operating voltages and $V_{turn\text{-}on}$ can be accounted for by a reduced injection barrier as well as higher electron mobility (μ_e) in ETL. As depicted in Figure 2a, there is a relatively large barrier of 0.4 eV for hole injection at NPB/TCTA contact (i.e., HOMO energies are 5.3 and 5.7 eV for NPB and TCTA) in the B/Y device. On the contrary, no injection barrier was observed for hole injection from NPB into the layer of yellow phosphor **Y-Pt** doped TCTA in the B/B/Y device due to direct injection/charge trap (further explained in Section 2.5), as shown in Figure 2c. In addition, BAlq with μ_e higher than that for TAZ (μ_e = 3.1 × 10^{-5} cm^2 V^{-1} s^{-1}[29] for BAlq and 1.3 × 10^{-5} cm^2 V^{-1} s^{-1}[30] for TAZ at the same electric field of 1.0 MV cm^{-1}) contributes to a lower driving voltage observed with the modified WOLEDs.

2.5. Mechanism for Performance Improvement

The efficiency enhancement by utilizing the modified device structure can be rationalized in terms of the high Φ_L (≈86%)

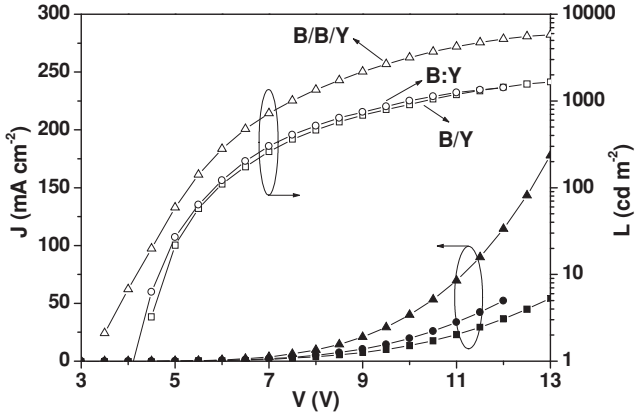

Figure 7. *J–V–L* characteristics of WOLEDs with various structures of ITO/MoO_x (5 nm)/NPB (40)/TCTA (5 nm)/2% **Y-Pt**:mCP (20 nm)/8% FIrpic:UGH2 (20 nm)/TAZ (40 nm)/LiF (0.5 nm)/Al (100 nm) (□), ITO/MoO_x (5 nm)/NPB (40 nm)/mCP (10 nm)/1% **Y-Pt**:8% FIrpic:UGH2 (20 nm)/TAZ (40 nm)/LiF (0.5 nm)/Al (100 nm) (○), and ITO/MoO_x (5 nm)/NPB (40 nm)/4% **Y-Pt**:TCTA (20 nm)/8% FIrpic:mCP (10 nm)/8% FIrpic:UGH2 (10 nm)/BAlq (40 nm)/LiF (0.5 nm)/Al (100 nm) (△).

of **Y-Pt** in the solid thin film and a broadened exciton formation–recombination region for blue emission. As previously mentioned, η_{WOLED} is controlled by η of monochromatic blue and yellow OLEDs. For the modified B/B/Y devices, the use of a higher content of **Y-Pt** (≈4%)—much closer towards its optimized value—would lead to more intense yellow emission in the EL spectrum and hence a higher η of yellow OLEDs. At the same time, the composite blue host could effectively broaden the exciton recombination zone of FIrpic blue phosphor as well as reduce the accumulation of triplet excitons at the emissive interface. Thus, the mechanism for the performance improvement can be elaborated by the energy level diagrams depicted in Figure 2. In general, triplet excitons can undergo radiative decay to give phosphorescence via two distinct pathways,[31] either by direct charge trapping on guest molecules (pathway 1) or by energy transfer from host to guest (pathway 2), depending on the concentration of guest molecules employed. The former pathway (i.e., pathway 1) has been proven to be more effective because excitons can be directly formed on guest molecule that avoids electrical excitation of the wide gap host, thereby eliminating exothermic back transfer from guest to host.[31] For the B/Y device (see Figure 2a), as the concentration of **Y-Pt** is low (≈2%), holes are expected to be injected from the hole-transporting TCTA layer into the HOMO of host layer mCP, where they combine with electrons to form triplet excitons at **Y-Pt** phosphor for yellow emission (via pathway 2). Meanwhile, holes will be directly injected into the FIrpic HOMO to give blue emission owing to the high concentration of FIrpic (≈8%) and the large injection barrier at the mCP/UGH2 interface (via pathway 1). It is important that the thickness of exciton formation zone (so-called "effective zone width") is strongly dependent on the phosphorescence lifetime of the triplet excited state of organometallic complexes.[32] Effective zone width is the optimized thickness of emissive layer that almost all excitons generated within the emissive layer can be used for light emission. Generally, the effective zone width is approximately equal to 10 nm for green emitters and becomes shorter for blue emitters with longer τ.[32,33] The long τ of FIrpic would limit the effective zone width (i.e., <10 nm) for efficient exciton formation. Further increase in blue emissive layer thickness would decrease the device performance in terms of η_{power}.

The present composite blue host of the modified WOLEDs can effectively broaden the exciton formation-recombination zone. In this work, this was composed of two different host materials, i.e., mCP and UGH2, each of 10-nm thickness and which were uniformly doped with 8% FIrpic. This can virtually extend the effective zone width for blue emission by two-fold, leading to significant decrease in accumulation of triplet excitons within the emissive layer in order to suppress triplet–triplet annihilation and to maximize η. It is noted that the modified B/B/Y architecture is different from that of the OLEDs with dual emissive layers previously reported in the literature.[34,35] The structures of the reported ITO/NPB/$Ir(ppy)_3$:TCTA/$Ir(ppy)_3$:$Bepp_2$/LiF/Al[34] and ITO/F_4-TCNQ:m-MTDATA/NPB/$Ir(ppy)_3$:TCTA/$Ir(ppy)_3$:BPhen/BPhen/LiF/Al[35] comprised at least one layer of either an ETL or a hole-transporting layer (HTL) doped with phosphorescent dopant(s). The performance improvement is attributed to the modulation of carrier mobility, leading to a better balance of hole and electron carriers. On the other hand, all the host materials used in the present devices show both intrinsically hole-transporting and electron-transporting properties.[36–38] Our present findings reveal that the phosphor concentration plays a crucial role in determining η of WOLEDs. The concentration should be high enough to increase the rate of triplet exciton transfer that leads to reduced triplet–triplet annihilation as well as to provide sufficient amount of luminescence sites for exciton formation and recombination in order to achieve high η_{yellow}. Employing a higher concentration of **Y-Pt** led to increased direct charge trapping at the **Y-Pt** site such that both energy transfer from the host to guest (i.e., **Y-Pt**) and radiative decay from the host became less prominent, thereby resulting in enhanced yellow emission from **Y-Pt**. This accounts for why further increase in the **Y-Pt** concentration—about twice the **Y-Pt** content in the modified WOLEDs—could lead to a significant enhancement of the performance of WOLEDs as revealed by the increase in total η_{power} from 45 lm W^{-1} for the 2% **Y-Pt** B/B/Y device to 61 lm W^{-1} for the 4% **Y-Pt** B/B/Y device.

3. Conclusion

In this work, WOLEDs with a modified structure consisting of a composite blue host for 8% FIrpic and a single yellow host for 4% **Y-Pt** have been fabricated. The composite blue host can effectively broaden the exciton formation zone as well as increases the intensity of yellow emission arising from higher concentration of **Y-Pt** employed. Particularly, the performance in terms of the total η_{power} and driving voltage at 1000 cd m^{-2} can be greatly improved from 31 lm W^{-1} and 10 V for control devices with conventional structures to up to 61 lm W^{-1} and 7.5 V. In addition, the efficiency roll-off at high brightness of 1000 cd m^{-2} has been reduced. These findings demonstrate the practical application of phosphorescent platinum(II) materials in OLED technology and that WOLEDs based on a blue and yellow approach incorporating a composite blue host could be a promising architecture in achieving high η used for solid-state lighting.

4. Experimental Section

Synthesis and Characterization of Complexes **1**–**5**: The O^N^C^N ligands were synthesized according to literature procedures[39,40] with the following sequence of (1) cadogan cyclization[41] (complexes **2** and **3**) or Friedel–Crafts acylation[42] (complexes **4** and **5**); (2) Ullmann reaction between 2-acetylcarbazole and 2-iodopyridine; (3) iodination of the Ketone in pyridine to α-pyridinium methyl ketone iodide; (4) Kröhnke annulation with α,β-unsaturated ketone. Subsequently, complexes **1**–**5** were done by refluxing the ligand with potassium tetrachloroplatinate(II) (K_2PtCl_4) in glacial acetic acid and chloroform.

1 (**Y-Pt**): ^{1}H NMR ($CDCl_3$, 500 MHz): δ9.97 (dd, J = 6.0 Hz, 1.3 Hz, H^1), 8.07 (s, 1H, H^{21}), 7.97-7.94 (m, 2H, H^4, H^{24}), 7.90 (d, J = 8.4 Hz, 1H, H^7), 7.87 (d, J = 7.4 Hz, 1H. H^{10}), 7.76 (t, J = 7.8 Hz, 1H, H^2), 7.64 (s, 1H, H^{32}), 7.59 (s, 2H, H^{30}), 7.51 (s, 1H, H^{19}), 7.45 (d, J = 8.0 Hz, 1H, H^{13}), 7.39 (t, J = 7.4 Hz, 1H, H^8), 7.36-7.31 (m, 2H, H^{14}, H^{26}), 7.26 (t, J = 7.4 Hz, 1H, H^9), 7.20 (dd, J = 8.3 Hz, 1.1 Hz, 1H, H^{27}), 6.83 (t, J = 6.2 Hz, 1H, H^3), 6.74 (t, J = 7.4 Hz, 1H, H^{25}), 1.49 (s, 18H, *t*-Bu). ^{13}C NMR ($CDCl_3$, 126 MHz): δ 164.76, 164.27, 153.13, 151.87, 150.21, 149.45, 149.39, 147.04, 142.74, 139.64, 138.29, 137.41, 136.85, 131.07, 130.09, 128.50, 126.17, 124.64, 124.23, 123.56, 122.78, 122.09, 121.47,

121.45, 118.75, 118.24, 117.58, 115.14, 114.55, 114.15, 113.62, 113.47, 35.18, 31.63.

2: ^{1}H NMR (CD_2Cl_2, 500 MHz): δ 10.06 (dd, J = 6.1 Hz, 1.5 Hz, 1H, H^1), 8.11 (s, 1H, H^{21}), 8.05 (d, J = 8.7 Hz, 1H, H^4), 8.00-7.97 (m, 2H, H^{10}, H^{24}), 7.91-7.88 (m, 2H, H^3, H^7), 7.67 (s, 1H, H^{19}), 7.65 (s, 3H, H^{30}, H^{32}), 7.61 (d, J = 8.0 Hz, 1H, H^{13}), 7.53-7.50 (m, 2H, H^8, H^{14}), 7.33 (t, J = 7.5 Hz, 1H, H^{26}), 7.19 (d, J = 8.4 Hz, 1H, H^{27}), 6.97 (t, J = 6.6 Hz, 1H, H^2), 6.72 (t, J = 7.5 Hz, 1H, H^{25}), 1.47 (s, 18H, *t*-Bu), 1.43 (s, 9H, *t*-Bu). ^{13}C NMR (CD_2Cl_2, 126 MHz): δ 165.49, 164.82, 153.62, 152.55, 150.96, 149.74, 147.84, 146.84, 143.06, 138.76, 138.41, 138.29, 137.62, 131.68, 130.70, 128.69, 125.04, 124.92, 124.84, 124.31, 123.77, 122.42, 122.05, 119.42, 118.76, 118.47, 118.14, 115.81, 115.07, 114.38, 114.14, 114.09, 35.63. 35.19. 31.99. 31.89.

3: ^{1}H NMR (CD_2Cl_2, 500 MHz): δ 10.13 (d, J = 5.9 Hz, 1H, H^1), 8.15 (s, 1H, H^{21}), 8.12 (d, J = 8.6 Hz, 1H, H^4), 8.06 (s, 1H, H^7), 8.03 (dd, J = 8.5 Hz, 1.4 Hz, 1H, H^{24}), 7.98 (t, J = 7.8 Hz, 1H, H^3), 7.93 (d, J = 8.2 Hz, 1H, H^{10}), 7.71 (s, 1H, H^{19}), 7.64 (s, 3H, H^{30}, H^{32}), 7.61 (d, J = 8.0 Hz, 1H, H^{13}), 7.56 (d, J = 8.0 Hz, 1H, H^{14}), 7.49 (dd, J = 8.2 Hz, 1.4 Hz, 1H, H^9), 7.33 (ddd, J = 8.3 Hz, 6.7 Hz, 1.5 Hz, 1H, H^{26}), 7.21 (d, J = 8.3 Hz, 1H, H^{27}), 7.04 (t, J = 6.5 Hz, 1H, H^2), 6.73 (ddd, J = 8.1 Hz, 6.7 Hz, 1.4 Hz, 1H, H^{25}), 1.49 (s, 9H, *t*-Bu), 1.46 (s, 18H, *t*-Bu). ^{13}C NMR (CD_2Cl_2, 126 MHz): δ 165.55, 164.82, 153.71, 152.54, 151.04, 150.05, 148.05, 142.84, 140.71, 138.66, 138.59, 137.92, 131.74, 130.71, 126.49, 125.00, 124.83, 124.31, 123.61, 122.44, 122.06, 121.59, 121.53, 119.51, 118.76, 118.36, 116.02, 115.18, 114.17, 111.59, 35.94, 35.63, 32.07, 31.88.

4: ^{1}H NMR (CD_2Cl_2, 500 MHz): δ 9.96 (d, J = 4.3 Hz, 1H, H^1), 8.16 (s, 1H, H^{21}), 7.96 (d, J = 8.3 Hz, 1H, H^{24}), 7.79-7.76 (m, 2H, H^3, H^{19}), 7.69 (d, J = 6.8 Hz, 1H, H^4), 7.63 (s, 3H, H^{30}, H^{32}), 7.54 (d, J = 8.0 Hz, 1H, H^{14}), 7.35 (t, J = 7.6 Hz, 1H, H^{26}), 7.25 (d, J = 8.4 Hz, 1H, H^{27}), 7.19 (d, J = 8.1 Hz, 1H, H^7), 7.16–7.05 (m, 3H, H^2, H^9, H^{10}), 7.04–6.98 (m, 1H, H^8), 6.87 (d, J = 8.2 Hz, 1H, H^{13}), 6.73 (t, J = 7.4 Hz, 1H, H^{25}), 1.44 (s, 18H, *t*-Bu). ^{13}C NMR (CD_2Cl_2, 126 MHz): δ 164.99, 164.52, 153.66, 152.60, 151.05, 150.52, 149.88, 148.72, 148.23, 141.11, 138.57, 137.65, 132.08, 131.90, 130.93, 129.72, 128.33, 126.39, 124.52, 124.35, 124.24, 123.20, 122.05, 121.75, 120.59, 118.84, 118.48, 118.32, 118.18, 115.43, 113.90, 111.19, 35.61, 31.84.

5: ^{1}H NMR (CD_2Cl_2, 500 MHz): δ 9.89 (dd, J = 6.2 Hz, 1.3 Hz, 1H), 8.18 (s, 1H, H^{21}), 7.97 (dd, J = 8.3 Hz, 1.6 Hz, 1H, H^{24}), 7.83 (s, 1H, H^{19}), 7.75 (ddd, J = 8.7 Hz, 7.1 Hz, 1.8 Hz, 1H, H^3), 7.63 (s, 3H, H^{30}, H^{32}), 7.53 (d, J = 8.0 Hz, 1H, H^{14}), 7.42–7.34 (m, 3H, H^4, H^8, H^{26}), 7.26 (dd, J = 8.4 Hz, 1.3 Hz, 1H, H^{27}), 7.16-7.13 (m, 4H, H^2, H^7, H^9, H^{13}), 7.06-7.00 (m, 1H, H^{10}), 6.74 (ddd, J = 8.2 Hz, 6.8 Hz, 1.4 Hz, 1H, H^{25}), 1.43 (s, 18H, t-Bu). ^{13}C NMR (CD_2Cl_2, 126 MHz): δ 165.02, 164.89, 153.73, 153.56, 152.63, 151.25, 148.25, 144.85, 144.38, 138.62, 138.47, 137.88, 132.00, 130.95, 130.84, 130.78, 129.10, 128.28, 126.25, 126.22, 124.45, 124.41, 123.63, 123.22, 122.38, 122.08, 122.05, 121.03, 119.30, 119.10, 115.49, 114.37, 35.61, 31.83.

^{1}H and ^{13}C nuclear magnetic resonance (NMR) spectra were recorded using $CDCl_3$ (**Y-Pt**) or CD_2Cl_2 (complexes **2**–**5**) as solvent on a Bruker Avance 500 FT-NMR spectrometer. Photo-excitation and emission spectra were obtained on a SPEX Fluorolog-3 spectrofluorometer. Emission lifetime measurements were performed with a Quanta Ray DCR-3 pulsed Nd:YAG laser system. Φ_L values were measured relative to that of a degassed acetonitrile solution of $[Ru(bpy)_3](PF_6)_2$ (Φ_{ref} = 0.062[43]) (**Y-Pt**, complexes **2** and **3**) or a benzene solution of 9,10-*bis*(phenylethynyl) anthracene (Φ_{ref} = 0.96[44]) (complexes **4** and **5**) as a standard reference. Energies of HOMO levels of the organic materials were estimated from their oxidation onset potentials determined by cyclic voltammetry, while those of LUMO levels were estimated by subtracting optical bandgaps from the corresponding HOMO energies. T_1 values were estimated from the peaks of the first vibronic bands/ the highest energy emission bands in the phosphorescence spectra recorded with 77 K 2-methyltetrahydrofuran frozen solutions. TGA was performed at a heating rate of 10 °C min^{-1} on a Perkin-Elmer TAC7/DX thermal analysis controller. Grace Reveleris iES Flash Chromatography system was employed to purify ligands of complexes and Reveleris Silica Flash Cartridge (size 40 g, Davisil@silica) was used as stationary phase.

OLED Fabrication: Photo-lithographically patterned ITO-coated glass substrates with sheet resistance of 20 ohm square^{-1} served as anode for OLEDs. Prior to thin-film deposition, glass substrates were routinely cleaned by ultrasonic bath in Decon 90 detergent and de-ionized (DI) water, and dried in an oven. They were then exposed to an ultraviolet-ozone environment before loading into an evaporation chamber. All organic and metal layers were sequentially grown in Trovato Mfg., Inc. vacuum deposition chamber at a base pressure of 10^{-6} Torr without vacuum break. Deposition rates were controlled to be 0.1–0.2 nm s^{-1} for all films and the film thicknesses were monitored in-situ using calibrated oscillating quartz-crystal sensors. Shadow masks for organics and metals were used to define organic and cathode patterns and to make four devices with the active emissive area of 0.1 cm^2 on each substrate. Except complexes **1**–**5**, all organic materials were purchased from Luminescence Technology Corp. or e-Ray Optoelectronics Technology Co. Ltd. and used as received without further purification. MoO_x and LiF were used as hole-injection[24,45] and electron-injection[46,47] materials, respectively, and purchased from Sigma-Aldrich Co. Details of each device structure are described in text.

OLED Characterization: *J*–*V*–*L* characteristics and EL spectra were measured simultaneously with a programmable Keithley model 2400 power source meter and a Photoresearch PR-655 spectroradiometer. All measurements for OLEDs were carried out without using any light out-coupling enhancement technique or an integration sphere. η_{EQE} was calculated from the forward viewing luminance, J, the EL spectrum and the photopic sensitivity of human eye by assuming a Lambertian distribution according to the literature.[6] All η mentioned in this work are η in forward viewing direction which are roughly equivalent to the total η measured in an integrating sphere divided by 1.7.[6,27]

Supporting Information

Supporting Information is available from the Wiley Online Library or from the author.

Acknowledgements

This work described in this paper was supported by the Innovation and Technology Commission of the HKSAR Government (GHP/043/10), Theme-Based Research Scheme (T23-713/11), and National Key Basic Research Program of China (No. 2013CB834802). This work was also supported by Guangdong Special Project of the Introduction of Innovative R&D Teams, China and Guangdong Aglaia Optoelectronic Materials Co., Ltd.

Received: January 24, 2013
Revised: March 21, 2013
Published online: May 2, 2013

[1] Y. Sun, N. C. Giebink, H. Kanno, B. Ma, M. E. Thompson, S. R. Forrest, *Nature* **2006**, *440*, 908.
[2] S. Reineke, F. Lindner, G. Schwartz, N. Seidler, K. Walzer, B. Lüssem, K. Leo, *Nature* **2009**, *459*, 234.
[3] H. Sasabe, J. I. Takamatsu, T. Motoyama, S. Watanabe, G. Wagenblast, N. Langer, O. Molt, E. Fuchs, C. Lennartz, J. Kido, *Adv. Mater.* **2010**, *22*, 5003.
[4] R. Wang, D. Liu, H. Ren, T. Zhang, H. Yin, G. Liu, J. Li, *Adv. Mater.* **2011**, *23*, 2823.
[5] C. L. Ho, W. Y. Wong, G. J. Zhou, B. You, Z. Xie, L. Wang, *Adv. Funct. Mater.* **2007**, *17*, 2925.
[6] S. L. Lai, S. L. Tao, M. Y. Chan, T. W. Ng, M. F. Lo, C. S. Lee, X. H. Zhang, S. T. Lee, *Org. Electron.* **2010**, *11*, 1511.

[7] S. L. Lai, Q. X. Tong, M. Y. Chan, T. W. Ng, M. F. Lo, S. T. Lee, C. S. Lee, *J. Mater. Chem.* **2011**, *21*, 1206.
[8] S. C. F. Kui, P. K. Chow, G. S. M. Tong, S. L. Lai, G. Cheng, C. C. Kwok, K. H. Low, M. Y. Ko, C. M. Che, *Chem. Eur. J.* **2013**, *19*, 69.
[9] D. P. K. Tsang, M. Y. Chan, A. Y. Y. Tam, V. W. W. Yam, *Org. Electron.* **2011**, *12*, 1114.
[10] X. Qi, M. Slootsky, S. Forrest, *Appl. Phys. Lett.* **2008**, *93*, 193306.
[11] W. Lu, B. X. Mi, M. C. W. Chan, Z. Hui, N. Zhu, S. T. Lee, C. M. Che, *Chem. Commun.* **2002**, 206.
[12] C. M. Che, S. C. Chan, H. F. Xiang, M. C. W. Chan, Y. Liu, Y. Wang, *Chem. Commun.* **2004**, 1484.
[13] B. P. Yan, C. C. C. Cheung, S. C. F. Kui, V. A. L. Roy, C. M. Che, S. J. Xu, *Appl. Phys. Lett.* **2007**, *91*, 063508.
[14] S. C. F. Kui, F. F. Hung, S. L. Lai, M. Y. Yuen, C. C. Kwok, K. H. Low, S. S. Y. Chui, C. M. Che, *Chem. Eur. J.* **2012**, *18*, 96.
[15] S. L. Lai, S. L. Tao, M. Y. Chan, M. F. Lo, T. W. Ng, S. T. Lee, W. M. Zhao, C. S. Lee, *J. Mater. Chem.* **2011**, *21*, 4983.
[16] T. Tsuzuki, N. Shirasawa, T. Suzuki, S. Tokito, *Adv. Mater.* **2003**, *15*, 1455.
[17] J. H. Yao, C. Zhen, K. P. Loh, Z. K. Chen, *Tetrahedron* **2008**, *64*, 10814.
[18] W. S. Huang, J. T. Lin, C. H. Chien, Y. T. Tao, S. S. Sun, Y. S. Wen, *Chem. Mater.* **2004**, *16*, 2480.
[19] Y. Tao, Q. Wang, C. Yang, K. Zhang, Q. Wang, T. Zou, J. Qin, D. Ma, *J. Mater. Chem.* **2008**, *18*, 4091.
[20] I. R. Laskar, S. F. Hsu, T. M. Chen, *Polyhedron* **2005**, *24*, 881.
[21] M. Li, W. H. Chen, M. T. Lin, M. A. Omary, N. D. Shepherd, *Org. Electron.* **2009**, *10*, 863.
[22] L. Xiao, Z. Chen, B. Qu, J. Luo, S. Kong, Q. Gong, J. Kido, *Adv. Mater.* **2011**, *23*, 926.
[23] Q. Wang, J. Ding, D. Ma, Y. Cheng, L. Wang, X. Jing, F. Wang, *Adv. Funct. Mater.* **2009**, *19*, 84.
[24] Irfan, M. Zhang, H. Ding, C. W. Tang, Y. Gao, *Org. Electron.* **2011**, *12*, 1588.
[25] M. A. Baldo, C. Adachi, S. R. Forrest, *Phys. Rev. B* **2000**, *62*, 10967.
[26] Y. Sun, S. R. Forrest, *Appl. Phys. Lett.* **2007**, *91*, 263503.
[27] B. W. D'Andrade, R. J. Holmes, S. R. Forrest, *Adv. Mater.* **2004**, *16*, 624.
[28] Commission Internationale de l'Eclairage. *Method of Measuring and Specifying Color Rendering Properties of Light Sources* (CIE 13.3.1995).
[29] J. W. Kang, D. S. Lee, H. D. Park, Y. S. Park, J. W. Kim, W. I. Jeong, K. M. Yoo, K. Go, S. H. Kim, J. J. Kim, *J. Mater. Chem.* **2007**, *17*, 3714.
[30] H. Sasabe, E. Gonmori, T. Chiba, Y. J. Li, D. Tanaka, S. J. Su, T. Takeda, Y. J. Pu, K. I. Nakayama, J. Kido, *Chem. Mater.* **2008**, *20*, 5951.
[31] R. J. Holmes, B. W. D'Andrade, S. R. Forrest, X. Ren, J. Li, M. E. Thompson, *Appl. Phys. Lett.* **2003**, *83*, 3818.
[32] S. Reineke, K. Walzer, K. Leo, *Phys. Rev. B* **2007**, *75*, 125328.
[33] S. J. Su, C. Cai, J. Kido, *Chem. Mater.* **2011**, *23*, 274.
[34] W. S. Jeon, T. J. Park, S. Y. Kim, R. Pode, J. Jang, J. H. Kwon, *Appl. Phys. Lett.* **2008**, *93*, 063303.
[35] X. Zhou, D. S. Qin, M. Pfeiffer, J. Blochwitz-Nimoth, A. Werner, J. Drechsel, B. Maennig, K. Leo, M. Bold, P. Erk, H. Hartmann, *Appl. Phys. Lett.* **2002**, *81*, 4070.
[36] T. Tsuboi, S. W. Liu, M. F. Wu, C. T. Chen, *Org. Electron.* **2009**, *10*, 1372.
[37] S. Noh, C. K. Suman, Y. Hong, C. Lee, *J. Appl. Phys.* **2009**, *105*, 033709.
[38] H. Fukagawa, N. Yokoyama, S. Irisa, S. Tokito, *Adv. Mater.* **2010**, *22*, 4775.
[39] S. J. Su, H. Sasabe, T. Takeda, J. Kido, *Chem. Mater.* **2008**, *20*, 1691.
[40] S. C. F. Kui, I. H. T. Sham, C. C. C. Cheung, C. W. Ma, B. Yan, N. Zhu, C. M. Che, W. F. Fu, *Chem. Eur. J.* **2007**, *13*, 417.
[41] A. W. Freeman, M. Urvoy, M. E. Criswell, *J. Org. Chem.* **2005**, *70*, 5014.
[42] H. Vanderhaeghe, *J. Org. Chem.* **1960**, *25*, 747.
[43] J. V. Caspar, T. J. Meyer, *J. Am. Chem. Soc.* **1983**, *105*, 5583.
[44] D. R. Maulding, B. G. Roberts, *J. Org. Chem.* **1969**, *34*, 1734.
[45] M. Y. Chan, S. L. Lai, K. M. Lau, M. K. Fung, C. S. Lee, S. T. Lee, *Adv. Funct. Mater.* **2007**, *17*, 2509.
[46] M. Y. Chan, S. L. Lai, C. S. Lee, S. T. Lee, *Chem. Phys. Lett.* **2003**, *380*, 298.
[47] L. S. Hung, C. H. Chen, *Mater. Sci. Eng. R* **2002**, *39*, 143.